






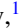





**Detailed study of multinucleon transfer features in the  $^{136}\text{Xe} + ^{238}\text{U}$  reaction**

E. M. Kozulin <sup>1,2</sup> G. N. Knyazheva <sup>1,2</sup> A. V. Karpov <sup>1,2</sup> V. V. Saiko <sup>1,3</sup> A. A. Bogachev <sup>1</sup>  
 I. M. Itkis <sup>1</sup> K. V. Novikov <sup>1,2</sup> I. V. Vorobiev <sup>1</sup> I. V. Pchelintsev <sup>1</sup> E. O. Savelieva <sup>1</sup>  
 R. S. Tikhomirov <sup>1</sup> M. G. Itkis<sup>1</sup> and Yu. Ts. Oganessian<sup>1,2</sup>

<sup>1</sup>*Flerov Laboratory of Nuclear Reactions, Joint Institute for Nuclear Research, 141980 Dubna, Russia*

<sup>2</sup>*Dubna State University, 141980 Dubna, Russia*

<sup>3</sup>*Institute of Nuclear Physics, 050032 Almaty, Kazakhstan*



(Received 30 October 2023; accepted 9 February 2024; published 21 March 2024)

**Background:** Multinucleon transfer (MNT) reactions are considered now as a possible tool to produce new isotopes of heavy and superheavy elements.

**Purpose:** Experimental study of MNT fragments formed in the  $^{136}\text{Xe} + ^{238}\text{U}$  reaction at  $^{136}\text{Xe}$  beam energy of 1.11 GeV and comparison with theoretical calculations.

**Methods:** Primary and secondary mass and energy distributions of projectilelike fragments (PLF) formed in the  $^{136}\text{Xe} + ^{238}\text{U}$  reaction have been experimentally investigated independently and in coincidence with survived heavy targetlike fragments (TLF) using the CORSET setup. Since the heavy fragments formed in the reactions are highly excited the masses, energies, and angles of both fragments as products of the sequential fission of heavy MNT fragments have been measured.

**Results:** The cross sections for PLFs at  $27.2^\circ \leq \theta_{\text{lab}} \leq 32.8^\circ$  along with survived TLFs and TLFs undergoing fission have been obtained. The mass loss during the deexcitation process of excited PLFs has been found using the measured primary and secondary masses. The excitation energies of light and heavy MNT fragments have been estimated from the mass loss and total kinetic energies. An overall good agreement with theoretical calculations increases reliability of performed analysis.

**Conclusions:** The transfer of about 27 nucleons from the projectile to target nucleus has been found. The cross section of the heaviest observed fragment with the mass of 265 u is about few hundred microbarns. The survival probabilities of transtarget nuclei formed in the reaction drop rapidly from  $\approx 7 \times 10^{-1}$  for the fragment mass of 240 u to  $\approx 1.8 \times 10^{-3}$  for 255 u.

DOI: [10.1103/PhysRevC.109.034616](https://doi.org/10.1103/PhysRevC.109.034616)

## I. INTRODUCTION

Present big success in the production of new superheavy nuclei has been achieved in the complete fusion reactions of two heavy nuclei [1]. However, the limitation to form more neutron-rich superheavy nuclei by complete fusion reactions with stable beams triggers the search for other superheavy element production approaches. The idea to produce the superheavy nuclei in the multinucleon transfer (MNT) reactions at the collision of uranium with actinides was proposed in the end of 1970's soon after the discovery of these processes [2–6]. In order to investigate the possibility of production of neutron-rich heavy actinide isotopes in such reactions the radiochemical study of the products formed in  $^{136}\text{Xe} + ^{238}\text{U}$ ,  $^{238}\text{U} + ^{238}\text{U}$ ,  $^{248}\text{Cm}$  collisions at interaction energies near the Coulomb barrier has been done [5–8]. It was found that the formation cross sections of trans-uranium elements decrease exponentially with increasing their atomic number, and for Fm isotopes it amounts a few microbarns [8]. Heavy isotopes of some trans-uranium elements  $^{254}\text{Cf}$ ,  $^{255}\text{Es}$ ,  $^{256}\text{Fm}$  [5] were produced in these reactions, which cannot be synthesized in complete fusion reactions with lighter ions.

During recent years it becomes more evident that MNT can be considered as the promising way to synthesize and investigate heavy and superheavy nuclei. This reaction leads

to the formation of two heavy fragments with full momentum transfer. The main part of the fragments, the so-called projectilelike and targetlike fragments, locates around the projectile and target masses, respectively.

In the collisions of heavy ions at energies near the Coulomb barrier, the potential energy surface determines strongly the evolution of the nuclear system, driving the interacting system in the direction of decreasing its potential energy in the multi-dimensional space of collective variables [9]. The appearance of the shell structure in potential energy can lead to an increase in the yield of MNT fragments in the regions of magic nuclei. In experimental study of mass-energy distributions of the fragments formed in the  $^{160}\text{Gd} + ^{186}\text{W}$  and  $^{88}\text{Sr} + ^{176}\text{Yb}$  reactions near the Coulomb barrier energies [10,11] the enhanced yield of products with masses around the closed shells at  $Z = 82$  and  $N = 82, 126$  was found supporting the important role of shell effects in MNT process. It was also shown that the orientation effect caused by the strong deformation of colliding nuclei can result in a gain in the yield of heavy targetlike fragments [11].

The transfer of nucleon clusters from projectile to the target nucleus is possible in MNT reactions, in which the ratio between the number of neutrons and protons varies over a very wide range. In addition, due to a significant dispersion in the

distribution of the excitation energy between complementary products, a heavy fragment can receive a noticeably lower excitation energy than in the case of nuclear fusion [2]. These properties of MNT reactions create favorable conditions for obtaining heavy isotopes of trans-uranium elements, which are of particular interest due to limited possibilities of their production in fusion reactions.

Recent theoretical calculations based on a multidimensional Langevin-type dynamical approach show that the formation of primary transtarget fragments in the reactions of heavy-ion beams with actinide targets are about a few millibarns [12]. However, due to a significant dissipation of initial interaction energy in MNT process the formed primary fragments have a large excitation energy. The fission barrier of these TLFs has mainly microscopic origin ( $B_f \approx 5$  MeV) and during the deexcitation process sequential fission occurs with high probability, whereas their survival after light particles evaporation is several orders of magnitude lower.

The radiochemical studies have shown that the yield of trans-uranium elements, especially their heavy isotopes, in reactions with uranium ions is 1–2 orders of magnitude higher than in the reactions with xenon ions [5,6,8]. Theoretical calculations [12,13] also suggest this observation—the nucleon transfer from projectile to target nuclei increases with increasing the projectile mass. The  $^{238}\text{U}$  ions are apparently the best bombarding particles in the synthesis of superheavy elements in MNT reactions.

However, the production of U beam is available in a few laboratories now. In this respect, extensive study of the reactions such as  $^{136}\text{Xe} + ^{238}\text{U}$  and  $^{209}\text{Bi} + ^{238}\text{U}$  can be very useful for deeper understanding of the MNT mechanisms and the best planning the future experiments on the production of new heavy isotopes in the reactions with  $^{238}\text{U}$  beam. Recently, the experimental study of a few nucleons transfer in the  $^{136}\text{Xe} + ^{238}\text{U}$  reaction at  $^{136}\text{Xe}$  energy of 1 GeV has been performed with PRISMA+AGATA setup [14]. It was found that population of neutron-rich actinide nuclei without proton transfer is indeed favored, and this type of reaction allows studying the nuclear structure of heavier actinides used as target material. Comparison of experimental mass distributions after multinucleon transfer with the GRAZING calculation yields has shown fair agreement for a few nucleons transfer channels. Analysis of the data has been rather complicated due to the large contribution of sequential fission fragments (SFF) originating in fission of excited MNT fragments.

Thus, since the sequential fission of TLFs is more probable than its survival after deexcitation process, the experimental identification of two fragments (PLF+TLF) and three fragments (PLF + both fragments of sequential fission of TLF) is needed. To explore the properties of MNT fragments such as their formation cross section, excitation energies, and survival probabilities, the primary and secondary mass and energy distributions of PLFs formed in the  $^{136}\text{Xe} + ^{238}\text{U}$  reaction at  $^{136}\text{Xe}$  beam energy of 1.11 GeV have been measured in coincidence with either survived TLFs or both fragments of sequential fission of excited TLFs. Our study was organized using two independent experimental techniques, namely, two-arm time-of-flight measurements (ToF-ToF method) to

TABLE I. The energy-dependent parameters of the reaction under study.  $E_{\text{lab}}$  is the beam energy,  $E_{\text{c.m.}}/E_C$  is the ratio of energy in the center-of-mass (c.m.) frame to the contact point potential,  $\theta_{\text{gr}}$  are the grazing angles in the laboratory (lab) and c.m. frames.

Parameter	
$E_{\text{lab}}$	1.11 GeV
$E_{\text{c.m.}}$	706.4 MeV
$E_{\text{c.m.}}/E_C$	1.48
$\theta_{\text{gr}} (^{136}\text{Xe})$ in c.m.	57.0°
$\theta_{\text{gr}} (^{136}\text{Xe})$ in lab	36.9°
$\theta_{\text{gr}} (^{238}\text{U})$ in lab	61.5°

investigate two-body coincidences and three-arm time-of-flight and energy measurements (ToF-E method) to investigate three-body coincidences. The energy-dependent parameters of the  $^{136}\text{Xe} + ^{238}\text{U}$  reaction are given in Table I.

## II. EXPERIMENT

The measurements were carried out using the U400 cyclotron at the Flerov Laboratory of Nuclear Reactions. The  $200 \mu\text{g}/\text{cm}^2$   $^{238}\text{U}$  target deposited on  $30 \mu\text{g}/\text{cm}^2$  carbon backing was irradiated with the 1.11 GeV  $^{136}\text{Xe}$  beam. The target backing faced the beam. The energy resolution of the beam was  $\approx 1\%$ . Beam ( $^{136}\text{Xe}^{47+}$ ) intensity on target was about 20 nA. The enrichment of the  $^{238}\text{U}$  target was 99.8%. The reaction products were measured using the CORSET spectrometer [15]. The scheme of the experimental setup is shown in Fig. 1.

Arm 1 of the spectrometer consists of a compact start and a position-sensitive stop detectors (indicated as St1 and Sp1 in Fig. 1) based on microchannel plates (MCP) with electrostatic mirrors for ToF measurements and  $E$  detector built as an assembly of 12 silicon detectors  $20 \times 20$  mm (SCD1 in Fig. 1).

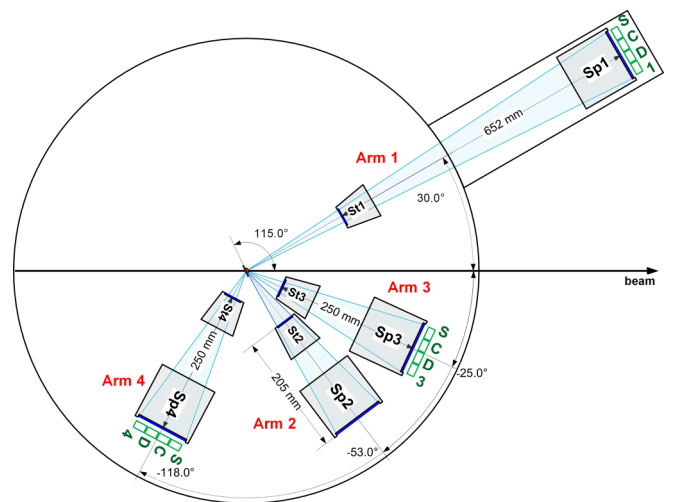


FIG. 1. The scheme of the experimental setup for investigation of two- and three-body kinematics in the  $^{136}\text{Xe} + ^{238}\text{U}$  reaction at  $E_{\text{lab}} = 1.11$  GeV.

The arm is located at an angle of  $+30^\circ$  with respect to the beam line and is intended to measure masses and energies of PLFs. The angular acceptance of the arm is  $\pm 2.8^\circ$  and  $\pm 2.1^\circ$  in and out of the reaction plane, respectively. Since the PLFs in this reaction have a relatively large velocity ( $\approx 3.5$  cm/ns), the ToF base is 652 mm to ensure the time resolution to be better than 1.5%.

Arm 2 (St2, Sp2 in Fig. 1), composed of the start and a position-sensitive stop MCP detectors, was installed at  $-53^\circ$  to measure the fragments complementary to PLFs in Arm 1. Its angular acceptances in and out of the reaction plane are  $\pm 7.4^\circ$  and  $\pm 5.5^\circ$ , respectively. The mean velocities of TLFs are about 1 cm/ns. The time resolution of the arm for the ToF distance of 205 mm is about 1%. The coincident measurements using Arms 1 and 2 allow us to investigate the mass and energy distributions of primary binary fragments formed in the reaction with full momentum transfer, whereas the secondary masses (after light particle evaporation), energies, and angles of PLFs are determined independently via ToF-E measurements by Arm 1.

Arms 3 and 4 are similar to Arm 1 and consist of the start, stop, and  $E$  detectors (St3, Sp3, SCD3 and St4, Sp4, SCD4 in Fig. 1). These arms are aimed to measure the masses, energies, and angles of fragments resulted from the sequential fission of TLFs. They are installed at  $-25^\circ$  and  $-118^\circ$ , which corresponds to the correlation angles of the two coincident fragments from TLF fission. Since such fragments have masses and energies in a typical fission range due to relatively small velocities of TLFs, the ToF distance of 250 mm provides a time resolution of about 2% and 1% for the Arms 3 and 4, respectively. The angular acceptance in and out of the reaction plane of Arm 3 is  $\pm 7.3^\circ$  and  $\pm 5.5^\circ$ , and  $\pm 7.6^\circ$  and  $\pm 5.7^\circ$  for Arm 4. The geometrical efficiency to detect both fragments of the sequential fission of TLF in coincidence with PLFs is about 1% and depends strongly on mass and energy of PLF.

The procedure of data processing for ToF-ToF and ToF-E measurements is described in Ref. [15]. In ToF-ToF method, the primary masses, velocities, energies, and angles of reaction products in the c.m. system are calculated from the measured velocities and angles using the momentum and mass conservation laws, assuming that the mass of the composite system is equal to  $M_t + M_p$  ( $M_p$  is the mass of projectile,  $M_t$  is the mass of target nucleus). The extraction of the binary reaction channels exhibiting full momentum transfer was based on the analysis of the kinematical diagram (see Ref. [15] for details).

The conversion foils of MCP start and stop detectors are made of 70- and 170  $\mu\text{g}/\text{cm}^2$  mylar films with a sputtered 30  $\mu\text{g}/\text{cm}^2$  gold layer. Corrections for fragment energy losses in the target material and in the foils of the detectors were applied in both methods.

All semiconductor detectors were calibrated using  $^{252}\text{Cf}$  source. No visible differences were found in the energy spectra collected before and after the beam time. Thus, the pulse height reduction was negligible during the experiment. The pulse height defect for  $E$  detectors found from the measurements of  $^{252}\text{Cf}$  spontaneous fission and elastically scattered  $^{136}\text{Xe}$  and  $^{238}\text{U}$  was taken into account.

### III. RESULTS AND ANALYSIS

#### A. Mass-energy distributions of PLF

The experimental mass-energy distributions of fragments formed in the  $^{136}\text{Xe} + ^{238}\text{U}$  reaction at  $E_{\text{lab}} = 1.11$  GeV and detected by Arm 1 are given in Fig. 2. The reconstruction of these distributions was based on ToF-E method. Since the measurements have been performed at angles a bit lower than the angles of grazing collisions (see Table I) elastic and quasielastic events located around mass of 136 u and c.m. energy of 450 MeV (the energy of elastically scattered  $^{136}\text{Xe}$  ion) are clearly pronounced in the mass-energy distribution. The elastic peak of the recoil target nucleus  $^{238}\text{U}$  is not visible in the spectra due to extremely low cross section at angles below the angle of grazing collisions for recoil nucleus ( $\theta_{\text{lab}} \approx 61.5^\circ$ ). The mass ( $\sigma_M$ ) and energy ( $\sigma_E$ ) resolutions of obtained spectra have been estimated from the width of distributions for these events and amount 2.9% and 1.9%, respectively.

Although the PLFs and SFFs of excited MNT fragments formed in the reaction have similar masses, they are distinguished well from each other by kinetic energies. The orange and gray contour lines indicate the location of MNT fragments (mainly PLFs) and SFFs in obtained mass-energy distribution [see Fig. 2(a)]. The kinetic energy distribution ( $E_{1\text{c.m.}}$ ) for PLFs is shown by open circles in Fig. 2(b). The contribution of elastic and quasielastic events is well described by Gaussian distribution (dash-dotted line). At the kinetic energies lower than 420 MeV it becomes insignificantly small. The events remaining after the subtraction of the Gaussian fit (solid circles), may be considered as MNT reaction products. The experimental cross section for MNT fragments integrated over azimuthal angles for the limited polar angles ( $27.2^\circ \leq \theta_{\text{lab}} \leq 32.8^\circ$ ) is  $810 \pm 50$  mb. The PLF cross sections are about 396 mb and 400 mb for the kinetic energy ranges  $300 \text{ MeV} \leq E_{1\text{c.m.}} \leq 420 \text{ MeV}$ , respectively. The cross sections are defined with respect to elastically scattered events.

The standard deviation of mass distribution  $\sigma_{M1}$  as a function of the kinetic energy of PLFs is presented in Fig. 2(c). The main trend is the decrease of  $\sigma_{M1}$  with increasing the fragment energy. For the kinetic energy range  $300 \text{ MeV} \leq E_{1\text{c.m.}} \leq 420 \text{ MeV}$  the dissipation of initial interaction energy is observed, whereas the mass transfer is relatively small (energy dissipation mode). For the fragments with kinetic energy lower than 300 MeV an increase of mass transfer is found. Such dissipation of the initial energy along with the mass transfer indicate a relatively long reaction time of about a few zeptoseconds in the Xe+U interaction [16].

Figure 2(d) shows the mass distribution for all fragments including SFFs with the kinetic energy lower than 420 MeV, the ones for the MNT fragments with energies lower than 300 MeV and within the range 300–420 MeV are presented in Fig. 2(e). One can see that for the MNT fragments with energies 300–420 MeV the mass yield peaks around 136 u and exponentially decreases with increasing the deviation from 136 u to lighter and heavier masses. It is a typical behavior for deep-inelastic collisions [2]. For the MNT fragments with energies lower than 300 MeV, in addition to a visible peak at 136 u, the smother decreasing of mass yield is found both

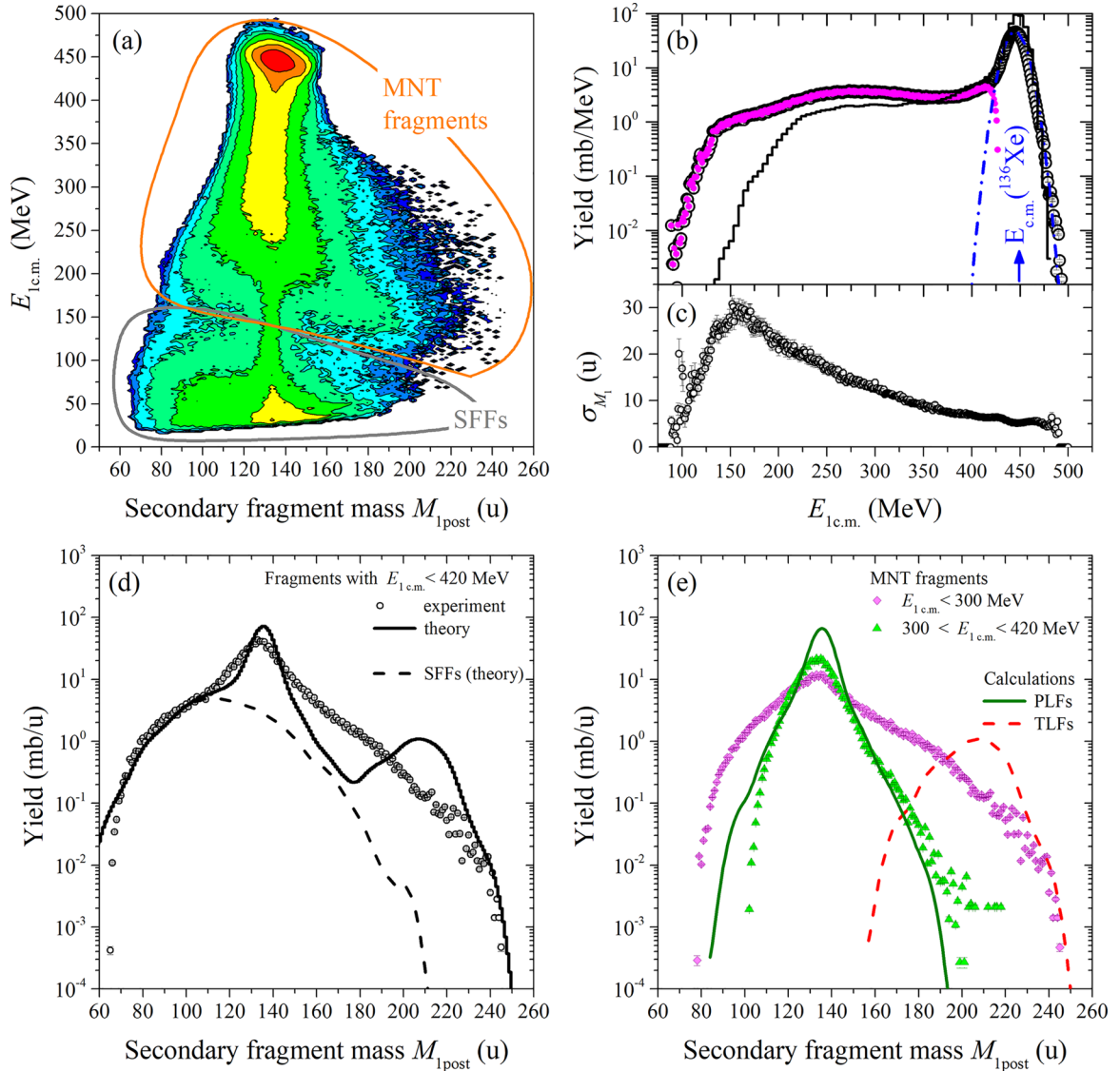


FIG. 2. The mass-energy distributions of fragments formed in the reaction  $^{136}\text{Xe} + ^{238}\text{U}$  at  $E_{\text{lab}} = 1.11$  GeV for  $27.2^\circ \leq \theta_{\text{lab}} \leq 32.8^\circ$ : (a) two-dimensional mass-energy distribution for all fragments, events inside the gray contour attributed to sequential fission of TLFs; (b) kinetic energy distribution of PLFs (open circles), the dash-dotted line is the Gaussian fit of elastic and quasielastic contribution, arrow indicates the energy of elastically scattered  $^{136}\text{Xe}$  ion; solid circles are the difference between the experimental data and the Gaussian fit, solid line is the theoretical calculation; (c) standard deviation of PLF masses  $\sigma_{M_1}$  in dependence on c.m. energies; (d) mass distributions of all fragments with kinetic energies lower than 420 MeV (open circles), lines are the theoretical calculations for all reaction products with kinetic energies lower than 420 MeV including SFFs (solid line) and for SFFs only (dashed line); (e) mass distributions for PLFs with  $E_{1.c.m.} < 300$  MeV (magenta rhombs) and  $300 \text{ MeV} \leq E_{1.c.m.} \leq 420$  MeV (green triangles), green solid and red dashed lines are the calculations for PLFs and TLFs.

for the fragments with masses lower than 136 u and for more symmetric fragments. A small amount of TLFs with masses 220–240 u is found. The yield of these events is of a few tens microbarns [see Figs. 2(a), 2(d)]. The cross section of the mass transfer to more symmetric fragment masses is about several hundred microbarns. Fragments with the masses heavier than  $A = 187$  probably can be formed via nucleon transfer from uranium to xenon. The larger mass transfer to more symmetric masses is caused by macroscopic potential of formed composite system  $^{136}\text{Xe} + ^{238}\text{U}$  favorable for symmetric fragment formation.

The obtained experimental results are compared with theoretical calculations performed within the framework of the dynamic model based on Langevin equations [17,18], which was applied to describe MNT processes in collisions with actinides. The lines in Figs. 2(b), 2(d), and 2(e) represent the predictions for the energy distribution of secondary MNT fragments formed in the studied reaction and their mass distributions. The experimental angular range as well as the experimental mass and energy resolution of 3.5 u and 10 MeV were taken into account in the calculations. According to the calculations, the total mass distribution shown in Fig. 2(d)

is comprised of three components corresponding to PLFs and TLFs [see Fig. 2(e)] as well as SFFs [dashed curve in Fig. 2(d)] scattered to this angular range. The mass distribution for the energy range  $300 \text{ MeV} \leq E_{\text{l.c.m.}} \leq 420 \text{ MeV}$  contains only the PLFs and agrees well with the corresponding experimental data. In the region of high energy losses, the model underestimates the cross section of deep inelastic collisions [Fig. 2(b)]. At the same time, the calculated mass distribution is higher than the experimental one in the region  $A = 200\text{--}240 \text{ u}$  [Fig. 2(d)]. According to the calculations, this is due to too high component of survived TLFs [Fig. 2(e)]. Such a high survival probability of TLFs may be caused by underestimation of the energy losses or excitation energies.

As it was already mentioned, the main interest in MNT reactions is connected with the possibility to produce new isotopes of heavy and superheavy nuclei. For this purpose, the nucleons have to be transferred from the lighter interacting nucleus to the heavy reaction partner. The formation cross section of the fragments lighter than  $136 \text{ u}$ , for which complementary fragments are trans-uranium nuclei, is about  $100 \text{ microbarns}$ . The lightest fragment mass found in the mass spectrum for PLF is  $82 \text{ u}$ . It should be noted that these masses are the secondary ones after the deexcitation process. Since the energy dissipation for these events is about a few hundred MeV, the mass loss occurring in deexcitation process of primary fragments should be taken into account to make the final conclusion about the heaviest product of the studied reaction.

### B. Primary mass-energy distribution of survived MNT fragments

The measured mass-total kinetic energy distribution ( $M$ -TKE) of MNT fragments formed in the  $^{136}\text{Xe} + ^{238}\text{U}$  reaction at angles  $44.7^\circ \leq \theta_{\text{lab}} \leq 61.3^\circ$  (Arm 2) is presented in Fig. 3. These fragments are complementary to PLFs with angles  $27.2^\circ \leq \theta_{\text{lab}} \leq 32.8^\circ$  (Arm 1).

In the heavy-ion-induced reactions, the difference between the reaction fragment angles in c.m. and laboratory frames is caused by a nonzero c.m. velocity of the formed composite system. For full momentum transfer, the folding angle (sum of both fragment angles) is  $180^\circ$  in the c.m. frame, whereas in the laboratory frame the folding angle changes depending on masses and energies of the reaction fragment pair. It leads to the different geometrical efficiencies of the fragment pairs due to the finite size of detectors [15]. In current measurements the detectors' geometry was chosen to achieve the maximal kinematic efficiency for the most probable mass and energies of surviving transtarget fragments. The reaction products with the masses and TKEs inside the gray region in Fig. 3 have zero efficiency in these experimental conditions. The elastically scattered  $^{136}\text{Xe}$  and  $^{238}\text{U}$  was excluded due to this geometry.

In the measured ToF1-ToF2 spectrum the contribution of events with full momentum transfer is about 23% from all collected events. The main part (77%) corresponds to SFFs. To separate these events the analysis of velocity components parallel and perpendicular to the beam axis has been applied. The details of such approach for the  $^{136}\text{Xe} + ^{208}\text{Pb}$  reaction is described in Ref. [19].

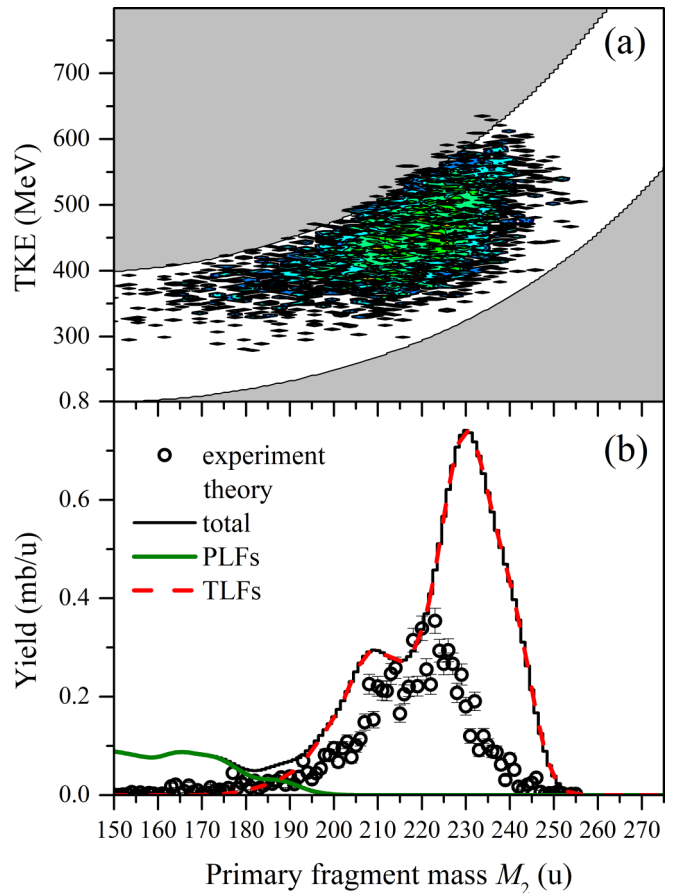


FIG. 3. (a) The  $M$ -TKE distribution of primary TLFs with full momentum transfer at  $E_{\text{lab}} = 1.11 \text{ GeV}$  for  $44.7^\circ \leq \theta_{\text{lab}} \leq 61.3^\circ$ , which are complementary to PLFs at  $27.2^\circ \leq \theta_{\text{lab}} \leq 32.8^\circ$  formed in the reaction  $^{136}\text{Xe} + ^{238}\text{U}$  (gray region indicates the area with zero geometrical efficiency of coincident fragments); (b) the experimental mass yield of TLFs (circles). Lines are the theoretical calculations.

The mass-energy distribution shown in Fig. 3(a) contains only the survived MNT fragments with full momentum transfer. The cross section of all events in this  $M$ -TKE matrix amounts to  $8.6 \pm 0.9 \text{ mb}$ . The most probable mass and TKE of TLFs are about  $222 \text{ u}$  and  $450 \text{ MeV}$ , respectively. The mean total energy losses  $\text{TKEL} = E_{\text{c.m.}} - \text{TKE}$  for these MNT fragments is about  $256 \text{ MeV}$ . The mass distribution predicted by theory for chosen experimental geometry is shown in Fig. 3(b). The calculation overestimates the yields of fragments heavier than  $225 \text{ u}$ . The two-humped structure in the mass distribution arises due to higher survival probability of fragments in the vicinity of the closed shells  $N = 126$  and  $Z = 82$ . The heaviest fragment mass found in the experimental  $M$ -TKE distribution is  $255 \text{ u}$  with the cross section of about  $2 \text{ } \mu\text{b}$ . Under the assumption of unchanged charge density of  $N/Z$  equilibration [20] giving a good approximation for primary fragments this mass corresponds to  $Z \approx 99\text{--}100$  (Es-Fm elements).

The average TKE for fragments from  $M$ -TKE matrix in Fig. 3(a) in dependence on MNT fragment mass is presented in Fig. 4. Measurements of the total kinetic energy of frag-

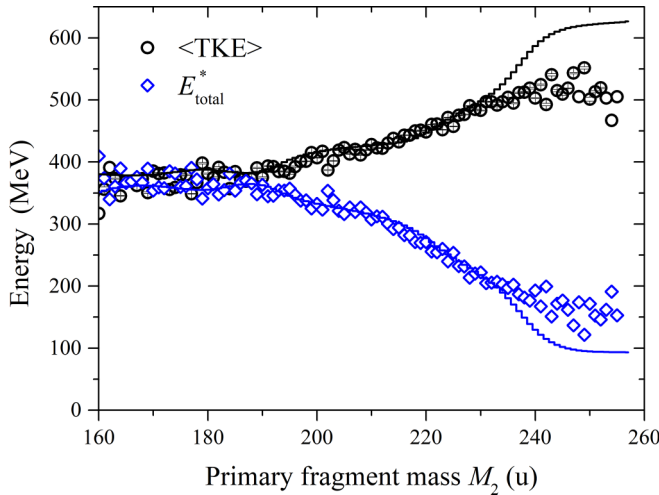


FIG. 4. The average TKE (circles) together with total excitation energy  $E_{\text{total}}^*$  (rhombs) as a function of primary fragment mass, solid lines are the theoretical calculations.

ments allow us to estimate the total excitation energy of the composite system formed in the reaction, part of which corresponds to the rotation energy of the fragments. According to the calculations, the average angular momentum of formed MNT fragments is about 30–40  $\hbar$  and their rotation energies amount approximately 6 MeV. The initial interaction energy  $E_{\text{c.m.}}$  is expended on the TKE of the fragments, the structural nucleon rearrangement of the formed MNT fragments ( $Q_{\text{gg}}$  value), deformation ( $E_{\text{def}}$ ), and the total excitation energy ( $E_{\text{total}}^*$ ):

$$E_{\text{total}}^* = E_{\text{c.m.}} - \text{TKE} + Q_{\text{gg}} - E_{\text{def}}. \quad (1)$$

The reaction  $Q_{\text{gg}}$  value may be estimated from measured MNT fragment masses as  $Q_{\text{gg}} = M_p + M_t - M_{\text{TLF}} - M_{\text{PLF}}$ . The deformation energy is transformed to the fragment excitation [21]. Therefore, the total excitation energy of the formed fragments may be estimated as:

$$E_{\text{total}}^* \approx E_{\text{c.m.}} - \text{TKE} + Q_{\text{gg}}. \quad (2)$$

The extracted total excitation energy is shown in Fig. 4. It is seen that nearly symmetric fragments are highly excited ( $E_{\text{total}}^* \approx 350$  MeV). For transtarget fragments the excitation is lower and amounts to about 150 MeV. The calculated average TKE and  $E_{\text{total}}^*$  are also given in Fig. 4. The theory agrees well up to the fragment mass  $\approx 230$  u, but for heavier fragments overestimates the  $\langle \text{TKE} \rangle$ , making, consequently, the distribution of the total excitation energies narrower with the lack of events corresponding to higher excitation energies (see Fig. 2 discussion). More certain conclusions concerning the observed discrepancy of the calculations and experimental data will require further analysis of the model both in its dynamical part determining characteristics of primary fragments as well as in the modelling the deexcitation of these fragments.

### C. Mass loss of PLF in deexcitation process

The deexcitation of the formed primary MNT fragments goes via emission of light particles. Since for the events de-

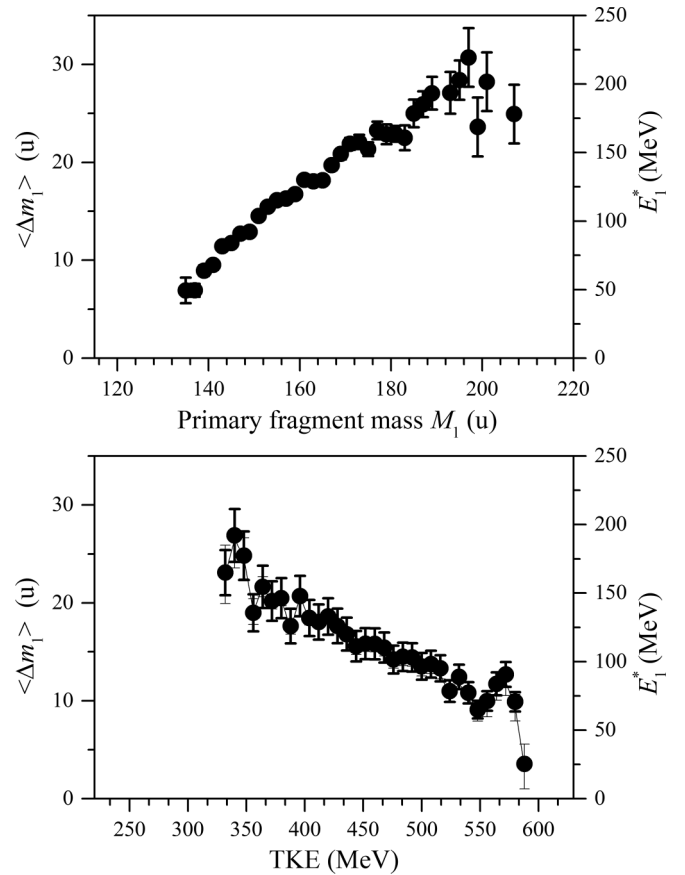


FIG. 5. The average mass loss ( $\Delta m_1$ ) (right scale indicates the corresponding excitation energy of the fragment) as a function of primary mass (top panel) and TKE (bottom panel) of MNT fragments.

tected in Arm 1 both the primary ( $M_1$ ) and the secondary ( $M_{1\text{post}}$ ) masses are measured, the mass loss  $\Delta m_1$  of MNT fragment occurring in deexcitation process can be found as the difference between these masses. Thus, an average mass loss  $\langle \Delta m_1 \rangle$  for each mass and TKE of the MNT fragment can be determined as

$$\langle \Delta m_1 \rangle (M_1, \text{TKE}) = \frac{1}{N} \sum_{i=1}^N (M_1^i - M_{1\text{post}}^i), \quad (3)$$

where  $N$  is the number of fragments at given mass  $M_1$  or/and TKE.

The uncertainty of the  $\langle \Delta m_1 \rangle$  value is defined as

$$\delta \langle \Delta m_1 \rangle = \sqrt{(\delta M_1^2 + \delta M_{1\text{post}}^2)/N}, \quad (4)$$

where  $\delta M_1$  and  $\delta M_{1\text{post}}$  are the experimental mass resolutions for ToF-ToF and ToF-E methods, respectively.

The average mass loss  $\langle \Delta m_1 \rangle$  as a function of mass and TKE of MNT fragment obtained with Eq. (3) is presented in Fig. 5. Notice that the mass loss can be found with Eq. (3) only for the events when both MNT fragments have been survived. The average mass loss increases linearly with increasing the fragment mass. The  $\langle \Delta m_1 \rangle$  dependence on TKE is opposite; the mass loss decreases when TKE increases. Such behavior is expected since the excitation is lower for higher TKE and,

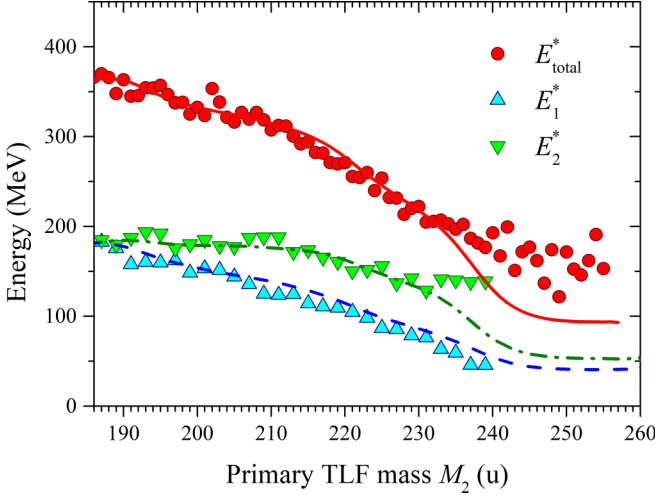


FIG. 6. The total excitation energy of the system  $^{136}\text{Xe} + ^{238}\text{U}$  after scission (red circles) and excitation energies of the light (blue up-triangles) and heavy (green down-triangles) fragments. Lines are the theoretical calculations.

therefore, smaller mass difference between primary and secondary fragments occurs.

Since the formed primary MNT fragments are neutron-rich nuclei, one may expect that their deexcitation goes mainly via neutron emission. Therefore, the excitation energy of fragment can be estimated using the obtained mass loss as

$$E_1^* = \langle \Delta m_1 \rangle (B_n + E_n), \quad (5)$$

where  $B_n$  is the neutron separation energy for MNT fragment,  $E_n$  is the kinetic energy of emitted neutron ( $E_n \approx 1.5$  MeV). The atomic number of fragments were not measured in this experiment. Therefore, the neutron separation energies were taken for the  $\beta$  stable nuclei for a given mass number in order to avoid additional assumption for the atomic number distribution of the MNT fragments. The right axes scales in Fig. 5 indicate the excitation energy  $E_1^*$  of the MNT fragment estimated with Eq. (5).

#### D. Excitation energies of light and heavy MNT fragments

The special interest in this study is connected with transtarget fragments. The excitation energy of these fragments after scission plays a crucial role in their survival probability. The estimated in the previous section excitation energy of light MNT fragments allows us to define the excitation of heavy ones:

$$E_2^* = E_{\text{total}}^* - E_1^*. \quad (6)$$

The total excitation energy and the excitation energies of heavy and light MNT fragments estimated from the measured  $\langle \text{TKE} \rangle$  and  $\langle \Delta m_1 \rangle$  are shown in Fig. 6 as a function of primary mass of the heavy fragment. The theoretically calculated excitation energies are also given. It is seen that the predicted excitation energy of the light MNT fragment is in a good agreement with the experimental one. The excitation energies of the heavy MNT fragments extracted from the experimental data are about 150–200 MeV. The predicted values for

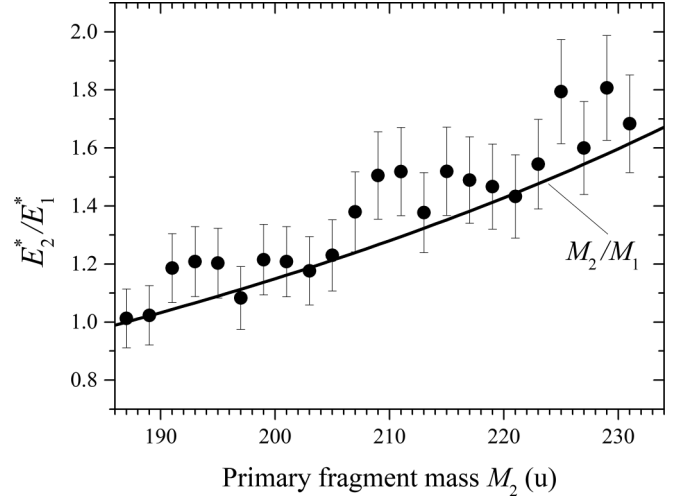


FIG. 7. The excitation energy ratio of heavy and light fragments as a function of primary mass of heavy MNT fragments. Line delineates the mass ratio of heavy and light fragments.

fragments with masses heavier than 230 u are lower than experimental one.

The division of the total excitation energy between formed fragments is an important point in our understanding of MNT process. If the interaction time is long enough to equilibrate the system, it is usually assumed that the excitation energy is divided between fragments proportionally to their masses [22]. However, the nonequilibrium division mode, according to which the excitation energy is divided approximately equally between fragments regardless of their mass, was also observed in grazing collisions of mass asymmetric nuclei [23]. This division regime transforms smoothly to the mass proportional one with increasing interaction time, so that the heavier fragment will take up more amount of the excitation energy in slower processes. Taking into account such a transition in the dynamic model made it possible to improve the description of MNT processes in mass asymmetric systems [24].

It is clearly seen in Fig. 7 that the ratio between excitation energies for heavy and light MNT fragments found from present analysis is proportional to their masses. Thus, it indicates that nonequilibrium division mode is negligible in this reaction, which is confirmed by the calculations.

#### E. Sequential fission of heavy MNT fragment

Since the MNT reaction is a binary process with full momentum transfer, the  $M$ -TKE distribution for all fragments (not only for survived ones) may be found for every PLF ( $M_{1\text{post}}$ ,  $E_{1\text{post}}$ ,  $\theta_1$ ,  $\varphi_1$ ) using the mass and momentum conservation laws. The mass and energy of PLFs have been corrected on the obtained average mass loss  $\langle \Delta m_1^* \rangle$  for those events where the corresponding TLFs undergo fission. The velocity vector diagram for an event of heavy MNT fragment sequential fission is schematically drawn in Fig. 8.

The velocity of center-of-mass system  $V_{\text{c.m.}}$  is defined as

$$V_{\text{c.m.}} = \frac{M_p V_p}{M_p + M_t} \quad (7)$$

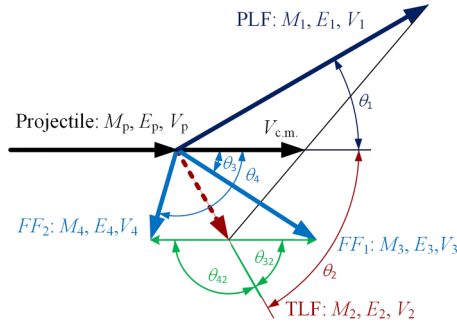


FIG. 8. The velocity vector diagram for heavy MNT fragment sequential fission events.

Thus, the mass ( $M_2$ ), velocity ( $V_{2c.m.}$ ), and the angles ( $\theta_{2c.m.}$ ,  $\varphi_{2c.m.}$ ) of TLF can be found:

$$M_2 = M_p + M_t - (M_{1post} + \langle \Delta m_1^* \rangle), \quad (8)$$

$$\theta_{2c.m.} = \pi - \theta_{1c.m.}, \quad (9)$$

$$V_{2c.m.} = \frac{(M_{1post} + \langle \Delta m_1^* \rangle)V_{1c.m.}}{M_2}. \quad (10)$$

The calculated values of  $\langle \Delta m_1^* \rangle$  are varying from 4.5 u to 6.5 u for the PLFs masses smaller than 130 u. The complementary TLFs are those which mainly contribute to the sequential fission events. Thus, keeping in mind some underestimation of the excitation energies by the theory, we used the constant value  $\langle \Delta m_1^* \rangle = 7$  u in the analysis of the experimental data. Eqs. (7)–(10) allow us to reconstruct the mass, velocity, and angles of the second fragment.

The angular distribution of the fission fragments would depend on the angular momenta of the primary TLFs, which align perpendicular to the reaction plane. Angular distributions of fission fragments formed in the  $^{16}\text{O} + ^{208}\text{Pb}$ ,  $^{232}\text{Th}$ ,  $^{238}\text{U}$  reactions at the compound nuclei excitation energies and angular momenta similar to those of the primary TLFs, formed in the studied reaction, were investigated experimentally in Ref. [25]. The obtained anisotropies  $A = W(0^\circ)/W(90^\circ) \approx 3.5$ . In the MNT-fragment rest frame, the fission fragments would have angular distribution similar to the one found in Ref. [25] and the most probable kinetic energy according to the Viola systematics [26]. Under these assumptions the efficiency of three-body event registration (Arm 1, Arm 3, and Arm 4 in coincidence) has been calculated as a function of mass and kinetic energy of the first fragment (PLF). The obtained efficiency is shown in Fig. 9.

Thus, at chosen geometry of the experiment the triple coincidence (PLF + 2 SFFs) may be detected for PLFs in the mass range 80–160 u with the kinetic energy higher than 150 MeV. This mass and energy range for PLFs corresponds to the main part of heavy MNT fragments where the sequential fission is highly probable.

### F. Data processing of three-body events

The Arm 3 measuring the SFF is installed at  $25^\circ$ . At this angle, elastic and quasielastic events together with PLFs give the main contribution, similar to the case of Arm 1 at  $30^\circ$

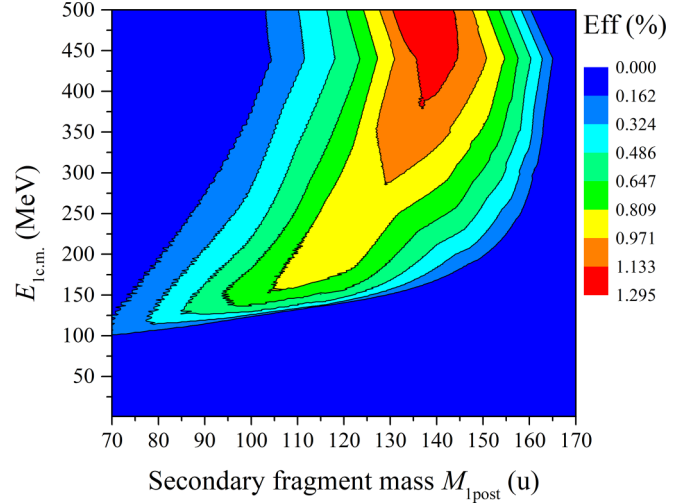


FIG. 9. The calculated geometrical efficiency (%) of three-body coincidence (Arm 1, Arm 3, and Arm 4) as a function of mass and kinetic energy of PLF.

[see Fig. 2(a)]. Contrary to Arm 3 and Arm 1, the main part of fragments detected by Arm 4 are the fragments of sequential fission of the heavy MNT product. The ToF3-ToF4 correlation allows separating SSFs from all other possible fragments formed in the reaction. From  $10^6$  events detected by Arm 3, only  $10^4$  events coincide with Arm 4. The total statistics of triple coincidences between Arm 1, Arm 3, and Arm 4 collected during the experiment is about  $10^3$  events. Moreover, each three-body event has to satisfy the velocity vector diagram given in Fig. 8.

From the measured masses, velocities, and angles of fission fragments of TLF, the velocities ( $V_{32}$  and  $V_{42}$ ) and angles ( $\theta_{32}$  and  $\theta_{42}$ ) can be found in the TLF rest frame. In the case of fission of heavy MNT fragment the obtained angles have to satisfy the conditions:

$$\theta_{32} + \theta_{42} = \pi; \quad \varphi_{32} + \varphi_{42} = \pi. \quad (11)$$

The excitation energies of fissioning TLFs are high and it is expected that the formed fission fragments will evaporate light particles during their deexcitation. The emission of each particle results in a small change in scattering angle, that leads to deviation from  $180^\circ$  in Eq. (11). In Fig. 10(a) the obtained folding angles  $\theta_{32} + \theta_{42}$  and  $\varphi_{32} + \varphi_{42}$  for all detected three-body events are shown. The main part of events is located around  $180^\circ \pm 10^\circ$  [events inside the red contour in Fig. 10(a)].

The TKE of fission fragments ( $\text{TKE}_{ff}$ ) can be also found event-by-event as

$$\text{TKE}_{ff} = E_{32} + E_{42}. \quad (12)$$

The most probable value of TKE may be estimated using the Viola systematics [26]. In Fig. 10(b) the  $\text{TKE}_{ff}$  obtained for all three-body events together with the Viola systematics in dependence on the mass of primary heavy MNT fragments undergoing fission is presented. The localization of folding angles around  $180^\circ$  and  $\text{TKE}_{ff}$  value close to the Viola systematics proves that the detected three-body events are formed



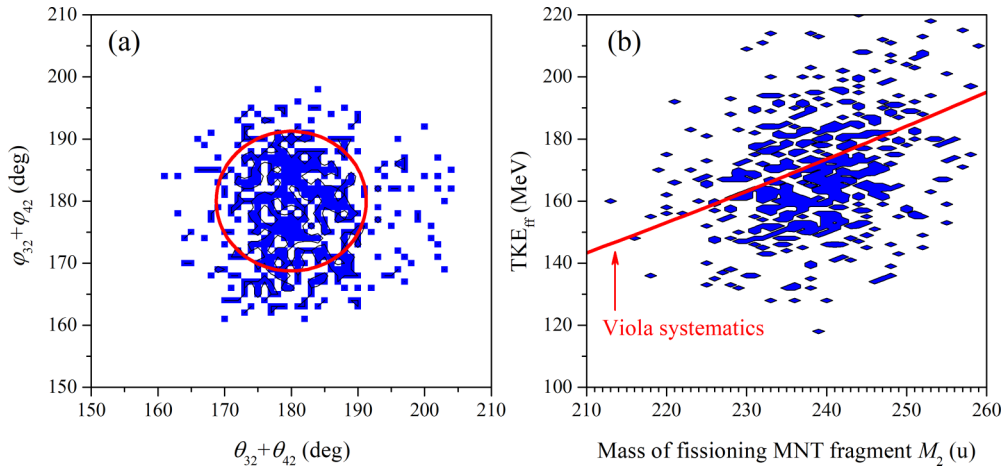


FIG. 10. (a) Folding angles distribution for SFFs extracted from the reconstruction of three-body events; (b) the TKE of fission fragments as a function of mass of heavy MNT fragments, red line delineates the Viola systematics.

as products of the two-stage process: the formation of MNT fragments in the Xe+U reaction and the sequential fission of excited heavy MNT fragments.

### G. Mass distribution of primary TLFs undergoing fission

The secondary mass distribution for PLFs corrected on geometrical efficiency of three-body coincidence (see Sec. III E), for the case when the coincidence with the both fragments of complementary TLF fission is detected, is shown in Fig. 11(a). The PLFs mass distribution for the case when the TLFs survive is also presented in Fig. 11(a). This mass distribution was found from the mass distribution of primary TLFs for  $44.7^\circ \leq \theta_{\text{lab}} \leq 61.3^\circ$ , which are complementary to PLFs at  $27.2^\circ \leq \theta_{\text{lab}} \leq 32.8^\circ$  (see Fig. 3) taking into account the kinematic efficiency due to the finite size of Arm 2 detectors. Since the arm was placed to optimize the regis-

tration of the heaviest transtarget nuclei with  $M_2 > 245$  u, the fragments with mass  $M_2 \approx 238$  u and  $TKE > 600$  MeV have been cut. The mass distribution for these fragments was restored as a difference between the mass distribution for all PLFs (see Fig. 2) and the one for three-body coincidence considering only the PLFs with TKE higher than the value where the efficiency is zero [the top gray region in Fig. 3(a)].

Using Eq. (8) the primary mass distribution for heavy MNT fragments complementary to PLF at  $27.2^\circ \leq \theta_{\text{lab}} \leq 32.8^\circ$  undergoing fission has been restored. The extracted mass distribution is shown in Fig. 11(b) together with the mass distribution for survived primary heavy MNT fragments. It is seen that for MNT fragments with masses heavier than 248 u the deexcitation process of formed excited MNT fragments mainly goes via their sequential fission. For fragments with masses around 255 u the survival probability against fission is only about  $1.8 \times 10^{-3}$ . The heaviest detected

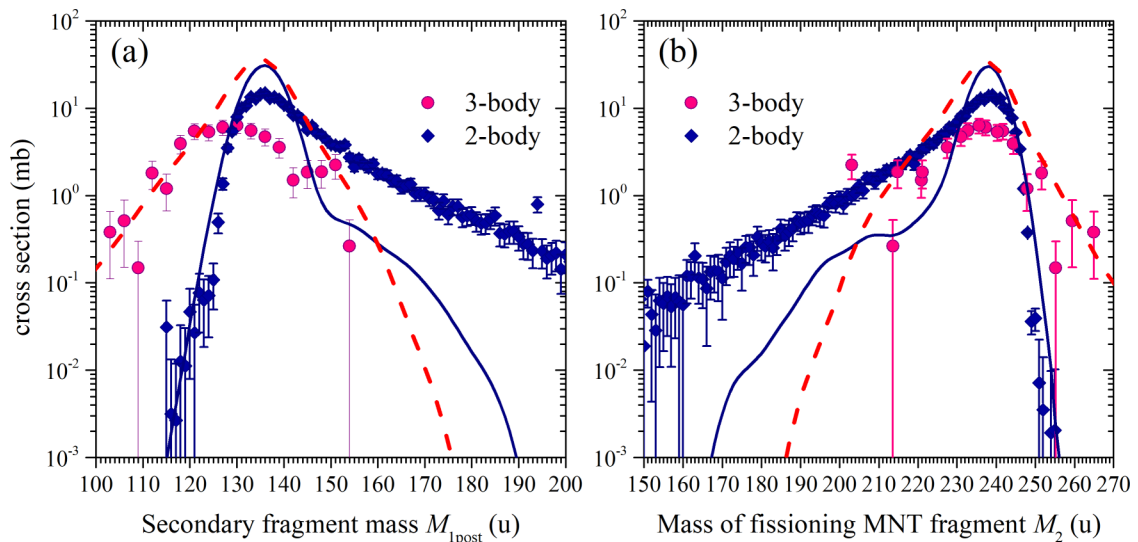


FIG. 11. (a) Mass distributions of secondary PLFs for two- and three-body coincidences (blue and pink symbols) at  $27.2^\circ \leq \theta_{\text{lab}} \leq 32.8^\circ$  formed in the  $^{136}\text{Xe} + ^{238}\text{U}$  reaction at  $E_{\text{lab}} = 1.11$  GeV; (b) mass distributions for primary TLFs for two- and three-body coincidences complementary to PLF at  $27.2^\circ \leq \theta_{\text{lab}} \leq 32.8^\circ$ . Lines are the theoretical calculations.

fragments originating in the collision of Xe and U are found in the mass spectrum for three-body events around the mass of 265 u that corresponds to  $Z \approx 103$  (Lr) under the assumption of unchanged charge density of  $N/Z$  equilibration [20].

The solid lines are the theoretical calculations of secondary mass distributions of PLFs at  $27.2^\circ \leq \theta_{\text{lab}} \leq 32.8^\circ$  [Fig. 11(a)] formed in the  $^{136}\text{Xe} + ^{238}\text{U}$  reaction at  $E_{\text{lab}} = 1.11$  GeV for the cases when the complementary TLFs survive and when they undergo sequential fission. The calculated primary mass distributions for survived and fissioning TLFs are shown in Fig. 11(b). The predicted mass yields for survived and suffering fission transtarget fragments are in good agreement with experimentally obtained spectrum.

#### IV. SUMMARY

To check the suitability of MNT reactions for production of new neutron-rich isotopes of heavy and superheavy nuclei, the mass, energy, and angular distributions of fragments formed in the  $^{136}\text{Xe} + ^{238}\text{U}$  reaction at the energy of  $^{136}\text{Xe}$  beam of 1.11 GeV were measured using modified CORSET setup. Installation of three independent ToF-E arms and additional ToF arm made it possible to study the properties of binary fragments, as well as three-body events (projectilelike fragment and sequential fission fragments of heavy MNT fragment).

Theoretical analysis of the reaction has been performed based on the Langevin-type dynamical model of nucleus-nucleus collisions. An overall reasonable agreement of theoretical calculations with the results of direct measurements and especially for some derived quantities, support experimental findings and increases reliability of performed analysis of the experimental data.

The total cross section of MNT fragments at  $27.2^\circ \leq \theta_{\text{lab}} \leq 32.8^\circ$  in the studied reaction is  $810 \pm 50$  mb. The main part of the fragments is located near the projectile mass. Nevertheless, the TLF fragments around the mass of 238 u with the cross section of about a few tens of microbarns

are revealed in the mass distributions. The lightest mass of secondary PLF is 82 u with the cross section of about 10  $\mu\text{b}$ .

The primary mass distribution of survived heavy fragments at  $44.7^\circ \leq \theta_{\text{lab}} \leq 61.3^\circ$ , which are complementary to PLFs at  $27.2^\circ \leq \theta_{\text{lab}} \leq 32.8^\circ$ , has a maximal yield at 222 u. The cross sections for heavier fragments decrease with increasing their masses. The heaviest survived fragments found in the present study are the isotopes of Es-Fm with the mass of 255 u and the cross section of about 2  $\mu\text{b}$ .

The measurements of TKE of the reaction fragments together with primary (via ToF-ToF) and secondary (via ToF-E) masses of projectilelike fragments allowed us to estimate the excitation energies of each fragment. It is found that the excitation energy divides proportionally to the fragment masses.

For the first time the measurements of three-body events formed in MNT reaction were carried out. It gave us the opportunity to restore the primary mass distribution of MNT fragments undergoing fission. The comparison of the primary mass distributions for survived and fissioning heavy MNT fragments has shown that the survival probabilities decrease with increasing their masses and the survival probability is about  $1.8 \times 10^{-3}$  for fragments with the mass of 255 u. The heaviest fragments observed in mass distribution of fissioning MNT fragments have the mass around 265 u (Lr isotopes) with the cross section of a few hundred microbarns. Thus, the transfer of about 27 nucleons from the projectile to the target nucleus is found in the present study.

#### ACKNOWLEDGMENTS

We thank the FLNR U400 accelerator team for the excellent beam quality, smooth operation of the cyclotron throughout the experiment, and friendly and professional attitude. Strong support of the directorate of the Flerov Laboratory of Nuclear Reactions is greatly acknowledged. This work was supported by the Grant No. 075–10–2020–117 from the Ministry of Science and Higher Education of the Russian Federation.

- 
- [1] Yu. Ts. Oganessian and V. K. Utyonkov, *Nucl. Phys. A* **944**, 62 (2015).
  - [2] V. V. Volkov, *Phys. Rep.* **44**, 93 (1978).
  - [3] K. D. Hildenbrand, H. Freiesleben, F. Pühlhofer, W. F. W. Schneider, R. Bock, D. v. Harrach, and H. J. Specht, *Phys. Rev. Lett.* **39**, 1065 (1977).
  - [4] H. Freiesleben, K. D. Hildenbrand, F. Pühlhofer, W. F. W. Schneider, R. Bock, D. v. Harrach, and H. J. Specht, *Z. Phys. A* **292**, 171 (1979).
  - [5] M. Schädel, J. V. Kratz, H. Ahrens, W. Brüchle, G. Franz, H. Gäggeler, I. Warnecke, G. Wirth, G. Herrmann, N. Trautmann, and M. Weis, *Phys. Rev. Lett.* **41**, 469 (1978).
  - [6] P. Glässel, D. v. Harrach, Y. Civelecoglu, R. Männer, H. J. Specht, J. B. Wilhelmy, H. Freiesleben, and K. D. Hildenbrand, *Phys. Rev. Lett.* **43**, 1483 (1979).
  - [7] R. J. Otto, M. M. Fowler, D. Lee, and G. T. Seaborg, *Phys. Rev. Lett.* **36**, 135 (1976).
  - [8] M. Schädel, W. Brüchle, H. Gäggeler, J. V. Kratz, K. Sümmerer, G. Wirth *et al.*, *Phys. Rev. Lett.* **48**, 852 (1982).
  - [9] V. Zagrebaev and W. Greiner, *Phys. Rev. Lett.* **101**, 122701 (2008).
  - [10] E. M. Kozulin, G. N. Knyazheva, S. N. Dmitriev, I. M. Itkis, M. G. Itkis, T. A. Loktev *et al.*, *Phys. Rev. C* **89**, 014614 (2014).
  - [11] E. M. Kozulin, V. I. Zagrebaev, G. N. Knyazheva, I. M. Itkis, K. V. Novikov, M. G. Itkis *et al.*, *Phys. Rev. C* **96**, 064621 (2017).
  - [12] V. Saiko and A. Karpov, *Eur. Phys. J. A* **58**, 41 (2022).
  - [13] V. I. Zagrebaev and W. Greiner, *Phys. Rev. C* **87**, 034608 (2013).
  - [14] A. Vogt, B. Birkenbach, P. Reiter, L. Corradi, T. Mijatovic, D. Montanari *et al.*, *Phys. Rev. C* **92**, 024619 (2015).
  - [15] E. M. Kozulin, A. A. Bogachev, M. G. Itkis, I. M. Itkis, G. N. Knyazheva, N. A. Kondratiev, L. Krupa, I. V. Pokrovsky, and E. V. Prokhorova, *Instrum. Exp. Tech.* **51**, 44 (2008).

- [16] W. W. Wilcke, J. R. Birkelund, A. D. Hoover, J. R. Huizenga, W. U. Schröder, V. E. Viola, K. L. Wolf, and A. C. Mignerey, *Phys. Rev. C* **22**, 128 (1980).
- [17] A. V. Karpov and V. V. Saiko, *Phys. Rev. C* **96**, 024618 (2017).
- [18] V. V. Saiko and A. V. Karpov, *Phys. Rev. C* **99**, 014613 (2019).
- [19] E. M. Kozulin, E. Vardaci, G. N. Knyazheva, A. A. Bogachev, S. N. Dmitriev, I. M. Itkis *et al.*, *Phys. Rev. C* **86**, 044611 (2012).
- [20] R. Vandebosch and J. R. Huizenga, *Nuclear fission* (Academic, Press New York, 1973).
- [21] C. Grégoire, C. Ngô, and B. Remaud, *Nucl. Phys. A* **383**, 392 (1982).
- [22] J. Wilczynski and H. W. Wilschut, *Phys. Rev. C* **39**, 2475 (1989).
- [23] R. Vandebosch, A. Lazzarini, D. Leach, D.-K. Lock, A. Ray, and A. Seamster, *Phys. Rev. Lett.* **52**, 1964 (1984).
- [24] V. Saiko and A. Karpov, *EPJ Web of Conf.* **223**, 01055 (2019).
- [25] B. B. Back, R. R. Betts, J. E. Gindler, B. D. Wilkins, S. Saini, M. B. Tsang, C. K. Gelbke, W. G. Lynch, M. A. McMahan, and P. A. Baisden, *Phys. Rev. C* **32**, 195 (1985).
- [26] V. E. Viola, K. Kwiatkowski, and M. Walker, *Phys. Rev. C* **31**, 1550 (1985).